Supplementary Information

Enhanced electrostatic shielding effect through incorporation of trace amounts of highly chelating anions for establishing a more stable electric double layer

Minghui Wang,[a] Junyi Yin,[a] Xiang Feng,[a] Fuxiang Li,[a] Zhuo Li,[a] Wen Zhang,[b] Yonghong Cheng,[a]* and Xin Xu[a]*

[a] State Key Laboratory of Electrical Insulation and Power Equipment, School of Electrical Engineering, Xi'an Jiaotong University, Xi'an 710049, PR China

[b] School of Chemistry, Xi'an Jiaotong University, Xi'an 710049, PR China

*Corresponding authors.

E-mail addresses: cyh@xjtu.edu.cn (Y. Cheng), xu.xin@xjtu.edu.cn (X. Xu).

Experimental Section

1. The Preparation of the Electrolyte

Pure $ZnSO_4$ electrolyte (2 mol L^{-1}) was prepared by dissolving 5751.2 mg of $ZnSO_4 \cdot 7H_2O$ (98%, Aladdin) into 10 ml of deionized (DI) water. The IDHA-x electrolyte (x=0.02 0.1 0.5) was prepared by adding 5751.2 mg of $ZnSO_4 \cdot 7H_2O$ and 3371*x mg of IDHA (AR, Aladdin) into 10 ml of deionized water (DI). The optimized concentration discussed in this paper is 0.02 mol L^{-1} and marked as "With IDHA", unless otherwise stated. And the "With Na_2SO_4" electrolyte was prepared by adding 5751.2 mg of $ZnSO_4 \cdot 7H_2O$ and 56.8 mg of Na_2SO_4 (99.5%, Tokyo Chemical Industry) into 10 ml of DI.

In order to research the chelating ability of IDHA anion, we prepared four different solution——Solution A (0.02 mol L^{-1} IDHA + 0.04 mol L^{-1} H_2SO_4), Solution B (0.04 mol L^{-1} Na_2SO_4), Solution C (0.02 mol L^{-1} IDHA + 0.04 mol L^{-1} H_2SO_4 + 2 mol L^{-1} $ZnSO_4$), and Solution D (0.04 mol L^{-1} Na_2SO_4 + 2 mol L^{-1} $ZnSO_4$) electrolytes were prepared in the similar process but replace DI to heavy water (99.9 atom % D, Meryer).

The electrolyte for Zn//δ-MnO_2 full cells were added with an extra 0.1 mol L^{-1} $MnSO_4$ (AR, Macklin).

2. Synthesis of Cathode Materials

The δ-MnO_2 were synthesized hydrothermally using $KMnO_4$ as reactants in aqueous solution [1]. 316 mg of $KMnO_4$ (AR, Sinopharm Chemical Reagent Co., Ltd) and 35 mL of DI water were mixed to form a uniform suspension. The mixture was

stirred and sonicated for 30 min and then transferred to a 50 mL Teflon-lined autoclave. The autoclave was placed in an oven at 180 °C for 3 h, and a brownish precipitate was collected via high-speed centrifugation at 8000 rpm. The precipitate was washed several times with DI water and ethanol and oven-dried at 60 °C to finally obtain theδ-MnO_2.

The $NH_4V_4O_{10}$ powders were synthesized by a hydrothermal method [2]. In detail, 0.585 g of ammonium vanadate (NH_4VO_3, 99%, Aladdin) was added into 35 mL DI water. Then 0.9455 g oxalic acid ($H_2C_2O_4 \cdot 2H_2O$, 99%, Meryer) powders were added into the NH_4VO_3 solution under magnetically stirring. The solution was transferred to a 50 mL Teflon-lined autoclave and heated at 140 °C for 12 h. After cooling, the products were collected by centrifugation and washed with DI water, then dried at 70 °C overnight to finally obtain the $NH_4V_4O_{10}$ powders.

3. The Preparation of the Electrode

For full batteries: The polished Zn foil was used as the anode. And preparing the cathode of a full cell by coating slurry made of cathode materials onto a stainless-steel foil. The slurry was prepared by mixing as-prepared active materials, super P, and polyvinylidene fluoride (PVDF) in a mass ratio of 7: 2: 1 with certain amounts of N-methyl-2-pyrrolidone (NMP). Then the working electrode was prepared by coating the slurry on the stainless foil and dried at 80 °C under vacuum for 12 h. The mass loading of the materials was about 1-2 mg cm^{-2}.

4. Characterizations

Scanning electron microscope (SEM; ZEISS, Gemini 500) was used to acquire the morphology of materials and elemental mapping images. X-ray diffraction (XRD) patterns were recorded by Bruker D8 Advance with a Cu Kα radiation (λ=1.54184 Å) from 5° to 90°. The solvation shells of Zn^{2+} and Na^{+} in various solutions were studied by liquid-state nuclear magnetic resonance (NMR; JNM-ECZ400S/L1) and Raman microscope (InVia Qontor).

5. Electrochemical Measurements

All testing CR2025-type coin cells were assembled in an open-air environment by using glass fiber filter (Whatman) as the separator. The electrolyte amount used in coin cells was 50 μL. The electrochemical performance of the batteries in this work was evaluated on a NEWARE CT-4008T battery test system. Symmetrical cells were fabricated by using two identical Zn foil (φ=16 mm, with thickness is 0.1 mm,). Zn//Cu half cells were assembled with Cu foil as the working electrode and Zn foil as the reference and counter electrode. Zn//MnO_2 or Zn//$NH_4V_4O_{10}$ full cells were assembled using Zn foil as anode and δ-MnO_2 or $NH_4V_4O_{10}$ as cathode. To assemble pouch cells, cathodes (3 × 3 cm^2) were coupled with the Zn anodes (3 × 3 cm^2). Glass fiber filter was used as the separator (4 × 4 cm^2).

For long-term cycling performance of Zn//Zn symmetric cells (x mA cm^{-2} y mAh cm^{-2}), constant current densities were applied as x mA cm^{-2} and the charging and discharging times were set to be $\frac{y}{x}$ h. For Zn//MnO_2 full cells, the voltage range was 0.8-1.8 V under different current densities (range from 0.5, 1, 2, 5, 10 A g^{-1}). For

Zn//$NH_4V_4O_{10}$ full cells, the voltage range was 0.8-1.8 V under different current densities (range from 1, 5A g^{-1})

The cyclic voltammetry (CV), linear scan voltammetry (LSV), corrosion test (TAF), chromoamperograms (CA), electrochemical impedance spectroscopy (EIS) and differential capacitance-potential curve were carried out on an electrochemical workstation (CHI 760E, CH Instruments, Ins) with a three-electrode system (For Zn//Cu half cells, Cu foil works as the working electrode and Zn foil as the reference and counter electrode). For Zn//MnO_2 full cells, CV was tested in the voltage range of 0.8-1.8 V (vs. Zn^{2+}/Zn) at a scan rate of 0.2 mV s^{-1}. For Zn//$NH_4V_4O_{10}$ full cells, CV was tested in the voltage range of 0.3-1.4 V (vs. Zn^{2+}/Zn) at a scan rate of 0.2 mV s^{-1}. Electric double layer capacitance (EDLC) measurements for CV curves of Zn//Zn symmetric cells at a scan rate of 8-16 mV s^{-1} between -15 to 15 mV, and calculated through the equation $C = i/v$ (C: capacitance; i: current. The value of i was determined by taking the half of the current difference between positive and negative scan under each scanning rate). LSV curves were measured at a scan rate of 2 mV s^{-1} from 0.05 V to -3 V (vs. Zn^{2+}/Zn). Tafel plots were measured by scanning between -0.15 and 0.15 V (vs. Zn^{2+}/Zn) at 2 mV s^{-1}. The CA tests were measured based on the Zn//Zn cell at a fixed overpotential of -150 mV. EIS spectra were recorded with a frequency ranging from 0.01 Hz to 10^5 Hz. The differential capacitance-potential curves were carried out through IMPE method in Zn//Cu cells at the frequency is 6 Hz and the amplitude (A) is 5 mV with potential ranging from 0.7 V to 0.1 V (vs. Zn/Zn^{2+}).

Supplementary Tables and Figures:

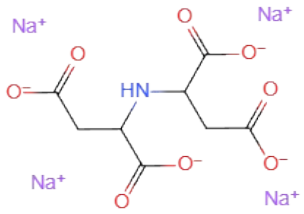

Fig. S1. The structure of EDTA (tetrasodium,2-(1,2-dicarboxylatoethylamino) butanedioate).

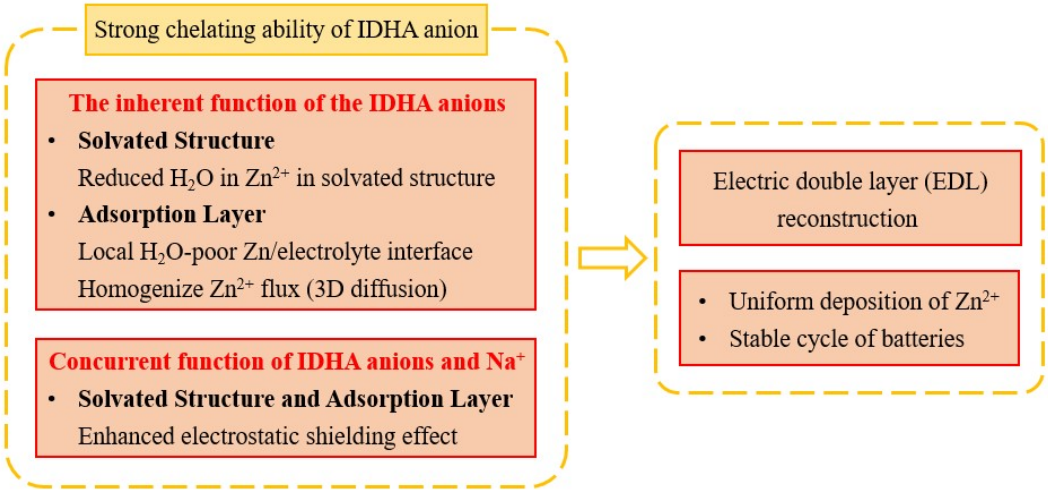

Fig. S2. Detailed schematic illustration of the multiple-function IDHA electrolyte.

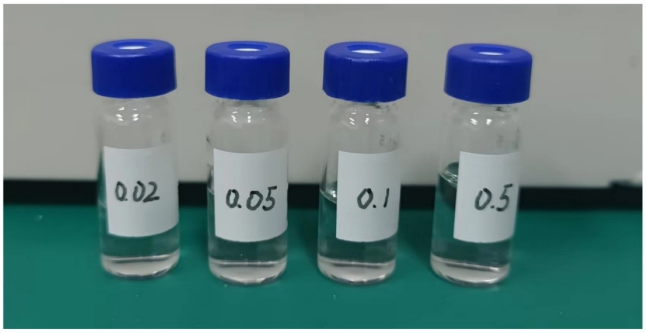

Fig. S3. Clear solutions of IDHA with four different concentrations (25 °C). This reveal the excellent water solubility and dispersibility of IDHA.

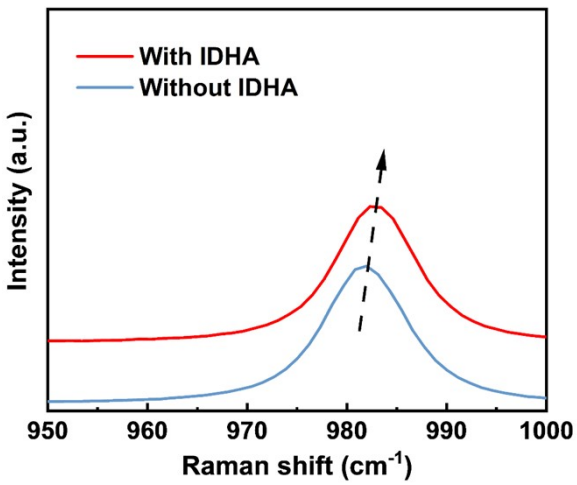

Fig. S4. The impact of IDHA usage on Raman spectroscopy. This phenomenon demonstrates the alteration of solvation structure by IDHA, but it remains unclear which ions' solvation structure undergoes changes.

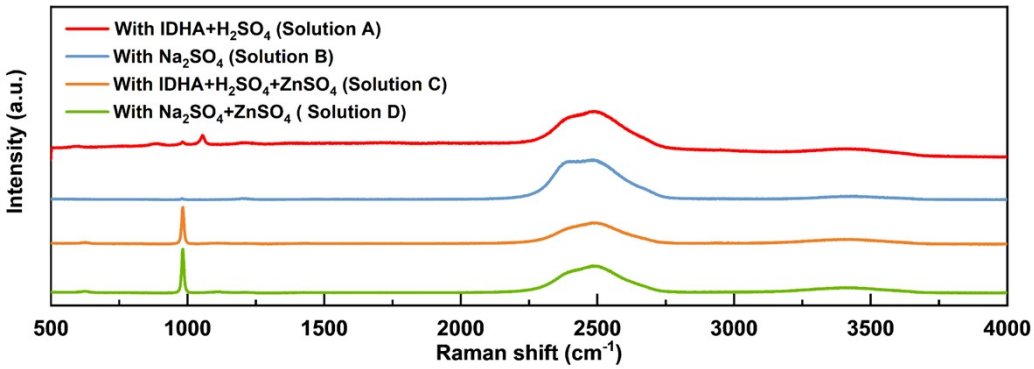

Fig. S5. Raman spectra of four different solutions——Solution A (0.02 mol L^{-1} IDHA + 0.04 mol L^{-1} H_2SO_4), Solution B (0.04 mol L^{-1} Na_2SO_4), Solution C (0.02 mol L^{-1} IDHA + 0.04 mol L^{-1} H_2SO_4 + 2 mol L^{-1} $ZnSO_4$), and Solution D (0.04 mol L^{-1} Na_2SO_4 + 2 mol L^{-1} $ZnSO_4$) with heavy water.

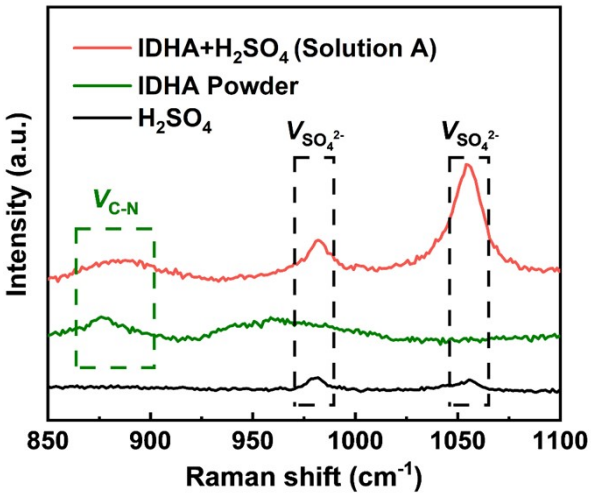

Fig. S6. Comparison of Raman spectra between Solution B, IDHA reagent, and H_2SO_4. It reveals that the three peaks in Solution B correspond to the C-N bond and sulfate groups, respectively.

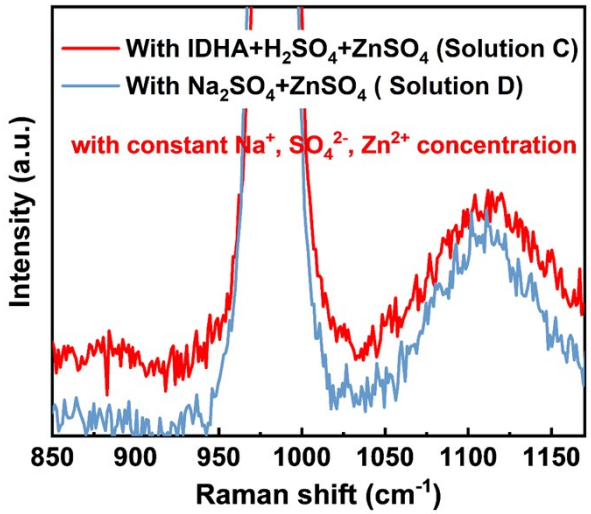

Fig. S7. Here is the enlarged spectrum for Figure 1g. This figure demonstrates that the peak at 1050-1200 cm^{-1} still exists in the Solution C and D, but its intensity is masked by the main peak near 980 cm^{-1}. Therefore, it can be proven that this peak corresponds to the SO_4^{2-}.

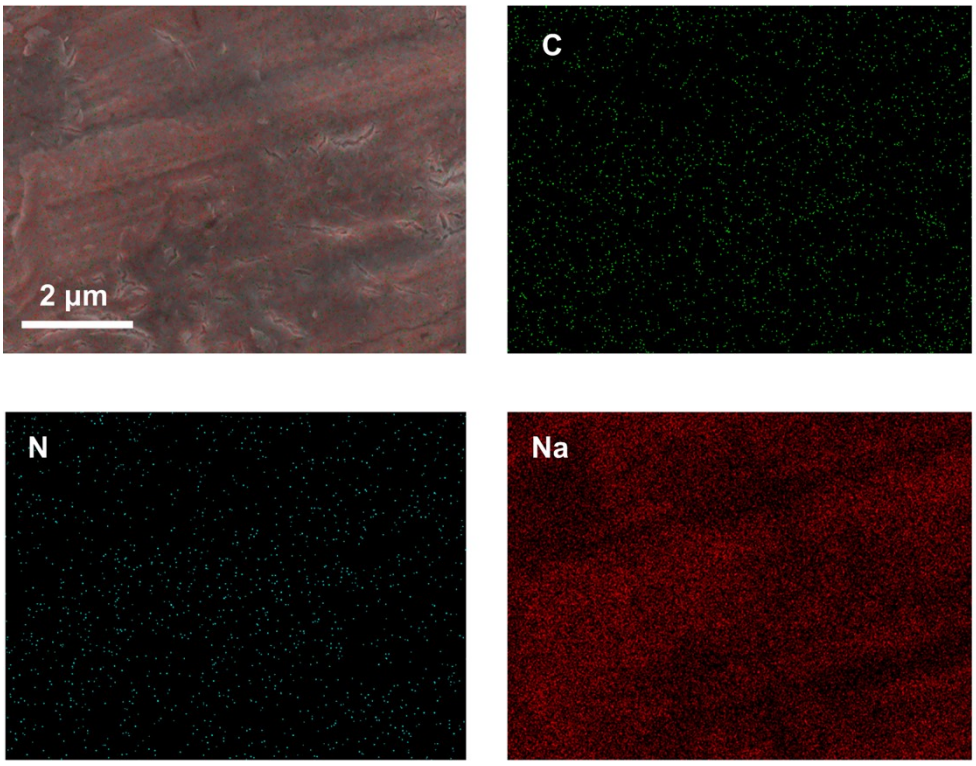

Fig. S8. EDS analysis of zinc foil after immersion in IDHA followed by rinsing.

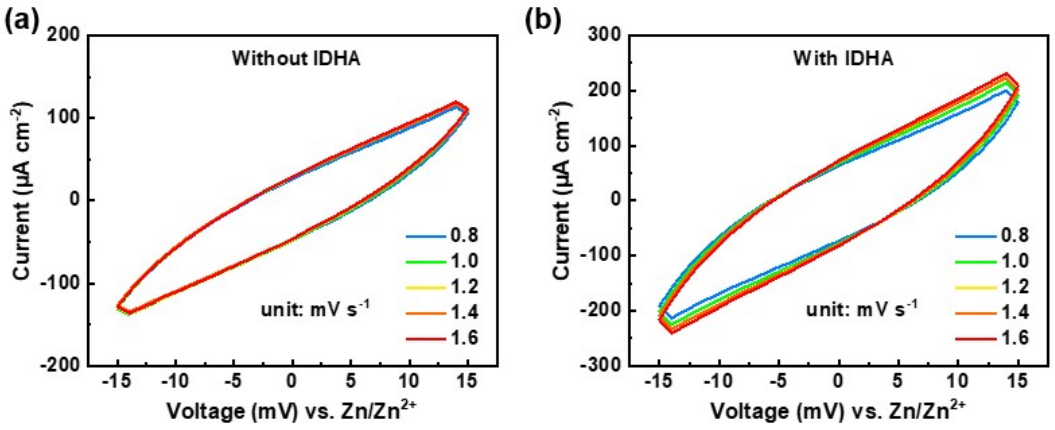

Fig. S9. CV curves of Zn//Zn symmetric batteries in a) $ZnSO_4$ and b) With IDHA electrolyte respectively.

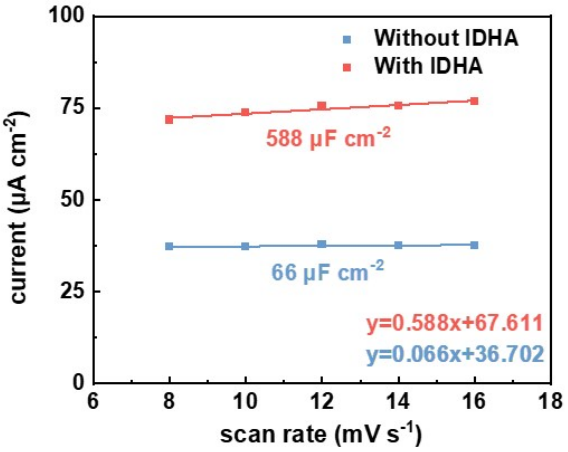

Fig. S10. EDL capacitance of Zn//Zn symmetric batteries with different electrolyte.

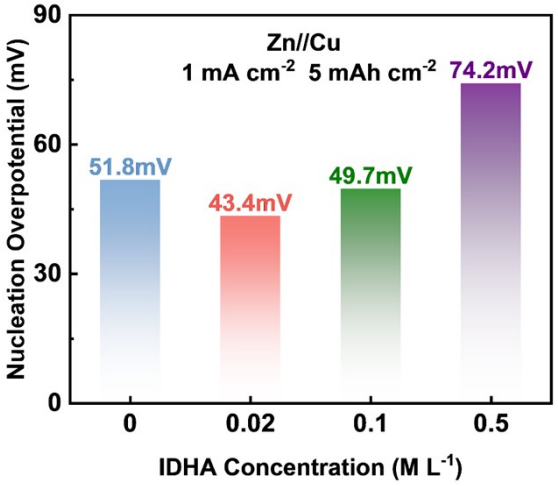

Fig. S11. Illustration of nucleation overpotential at various concentrations.

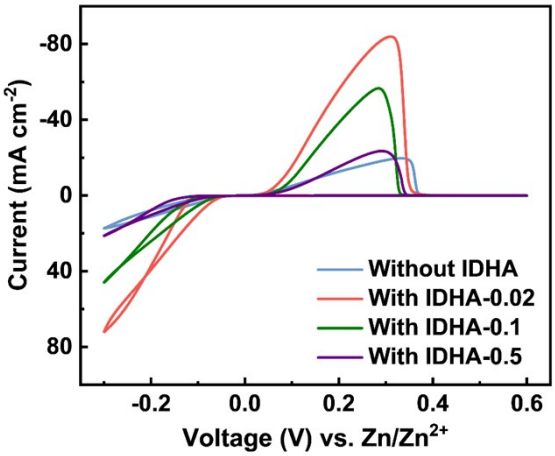

Fig. S12. Nucleation overpotential measured after assembling Zn//Cu asymmetric cells with different concentrations of IDHA additive.

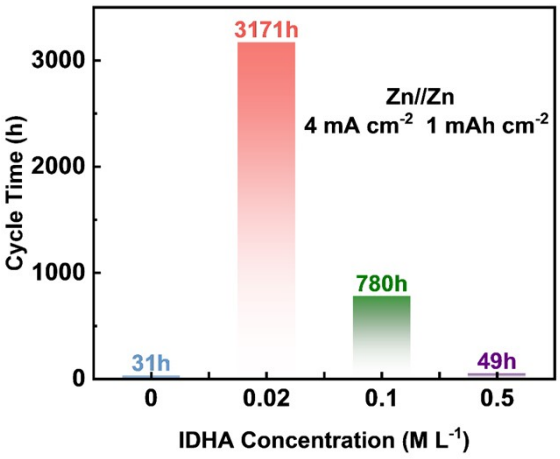

Fig. S13. Comparison of the cycling duration of Zn//Zn symmetric cells with different concentrations of IDHA at a current density of 4 mA cm^{-2} and 1 mAh cm^{-2}.

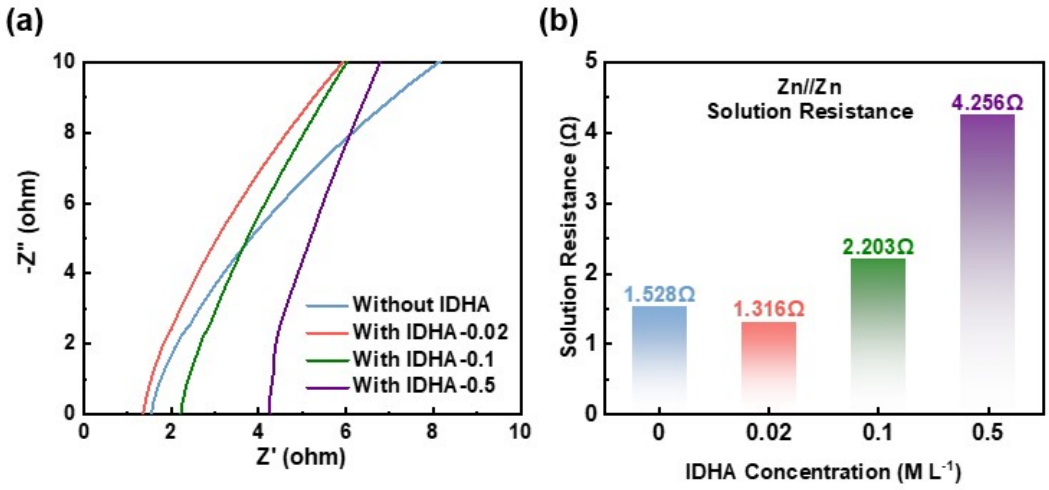

Fig. S14. (a) Locally magnified Nyquist plots of the Zn//Zn symmetrical cells in electrolytes adding different concentrations of IDHA (b) solution resistance for each system

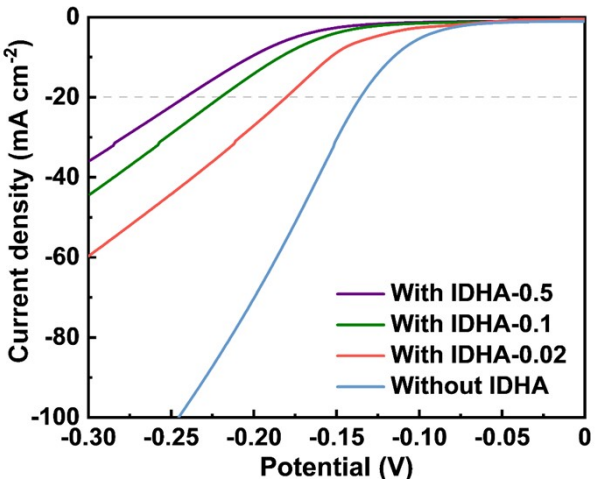

Fig. S15. The influence of different concentrations of IDHA on the hydrogen evolution performance (tested via linear sweep voltammetry).

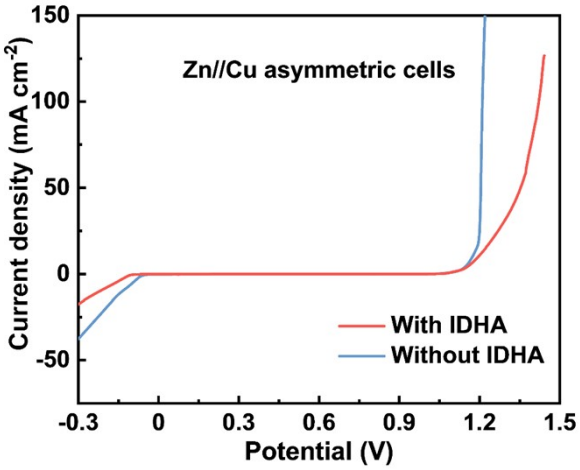

Fig. S16. The electrochemical stable window (ESW) measured for Zn//Cu asymmetric batteries.

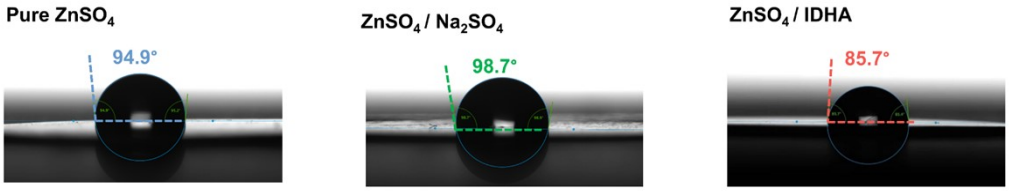

Fig. S17. Contact angles of three electrolytes with zinc foil.

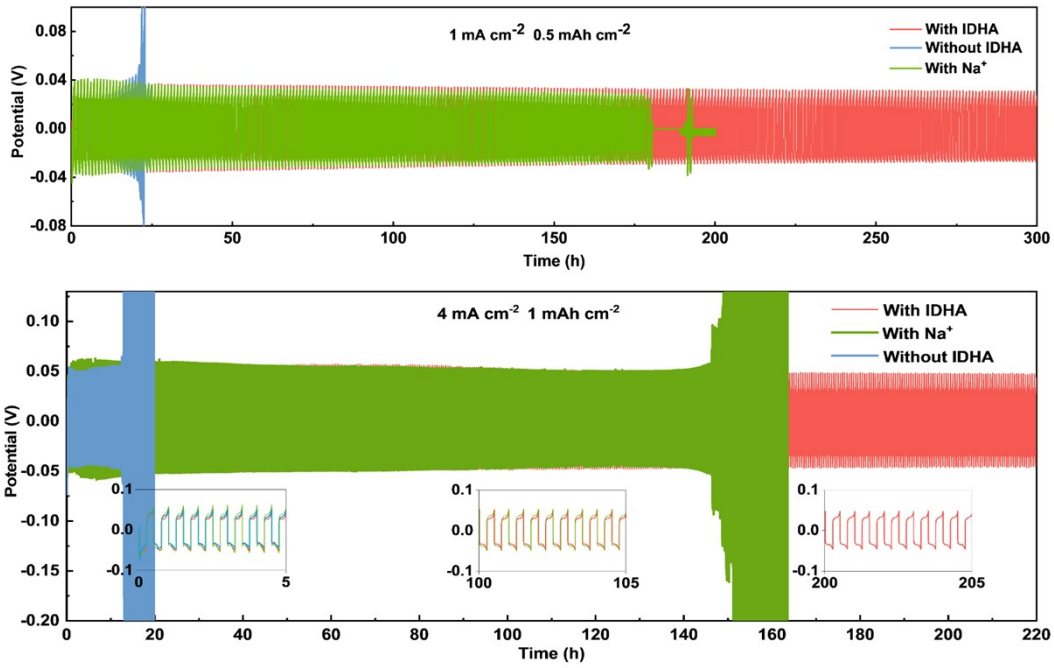

Fig. S18. Time-voltage curves of Zn//Zn symmetric cells with different electroyte during cycling at a current density of 1 mA cm^{-2} and 0.5 mAh cm^{-2} ,4 mA cm^{-2} and 1 mAh cm^{-2}.

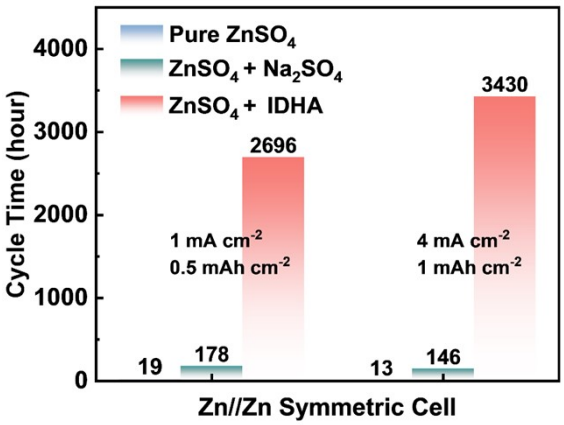

Fig. S19. Comparison of the cycling duration of Zn//Zn symmetric cells with different electroyte at a current density of 1 mA cm^{-2} and 0.5 mAh cm^{-2} ,4 mA cm^{-2} and 1 mAh cm^{-2}.

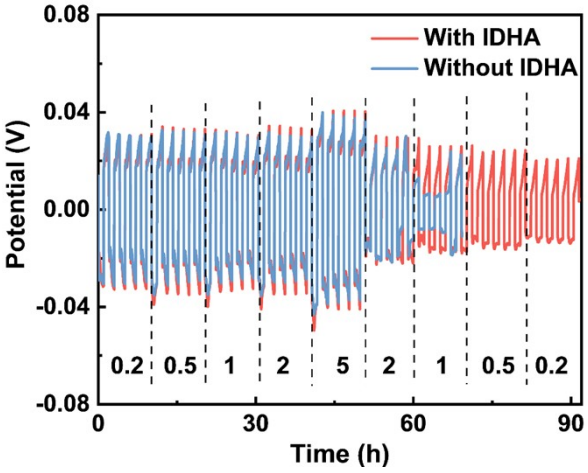

Fig. S20. Rate performance testing of Zn//Zn symmetric cells.

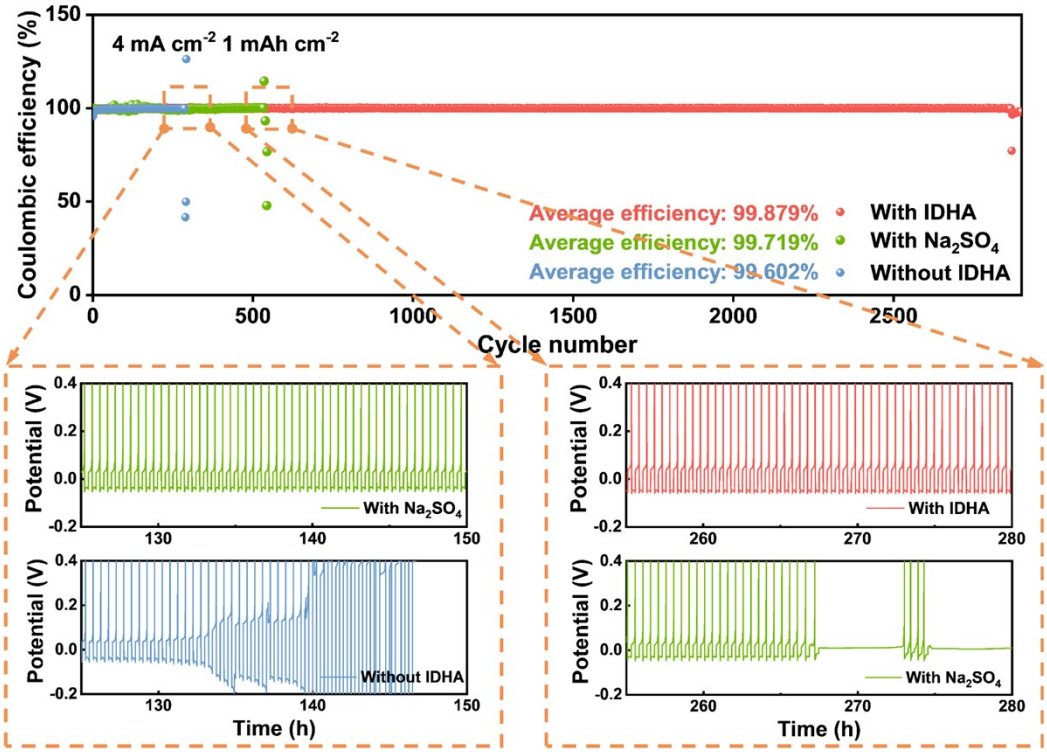

Fig. S21. Schematic of coulombic efficiency for Zn//Cu asymmetric cells with different electrolyte compositions, as well as time-voltage curves at the break point.

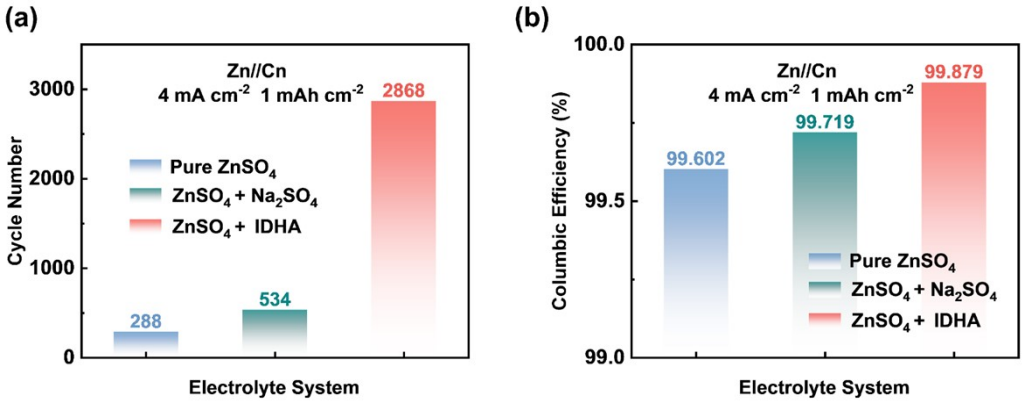

Fig. S22. Comparison of (a) the maximum cycle numbers and (b) coulombic efficiency for Zn//Cu asymmetric cells with different electrolyte compositions.

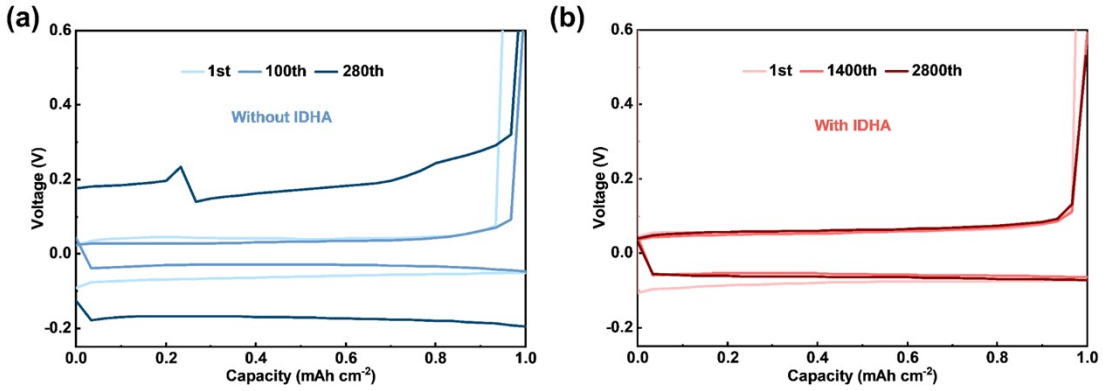

Fig. S23. The impact of adding IDHA on the capacity-voltage curve of Zn//Cu asymmetric cells. (4 mA cm^{-2}, 1 mAh cm^{-2}).

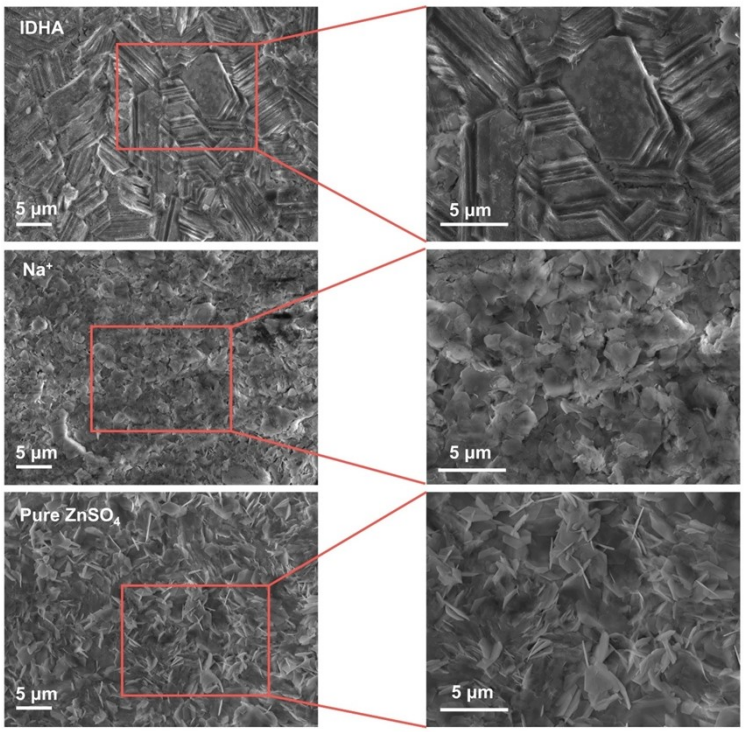

Fig. S24. Optical image of Zn electrode from the Zn//Zn symmetric cell after 10 cycles (1 mA cm^{-2}, 1 mAh cm^{-2}).

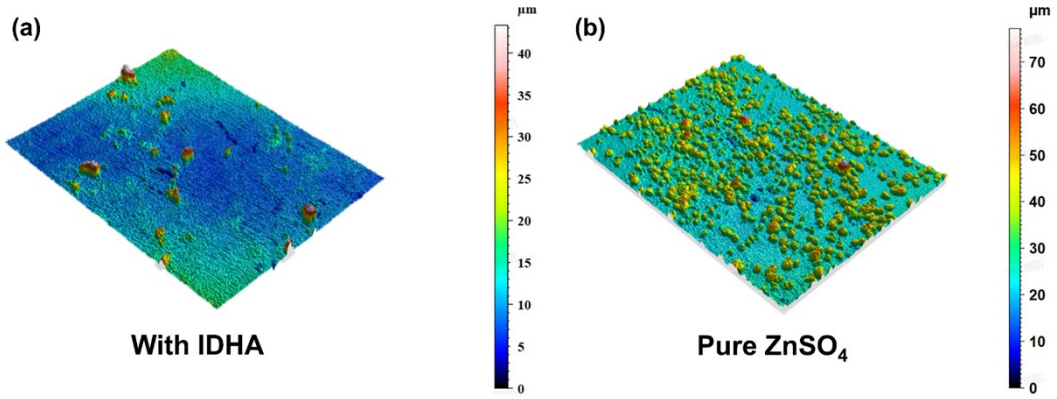

Fig. S25. Roughness after cycling 10 cycles at a current density of 5 mA cm^{-2}, 1 mAh cm^{-2}.

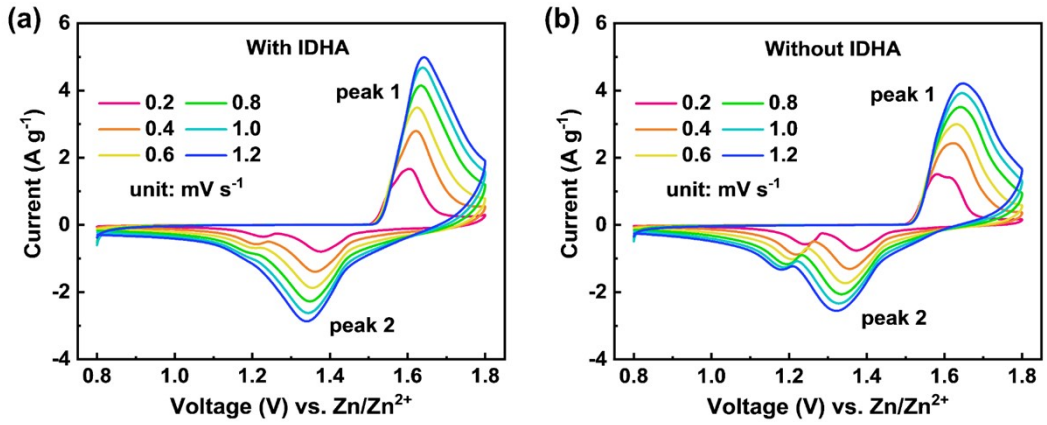

Fig. S26. CV test for Zn//δ-MnO_2 full-cells with different scan rate (0.2, 0.4, 0.6, 0.8, 1.0, 1.2 mV s^{-1}).

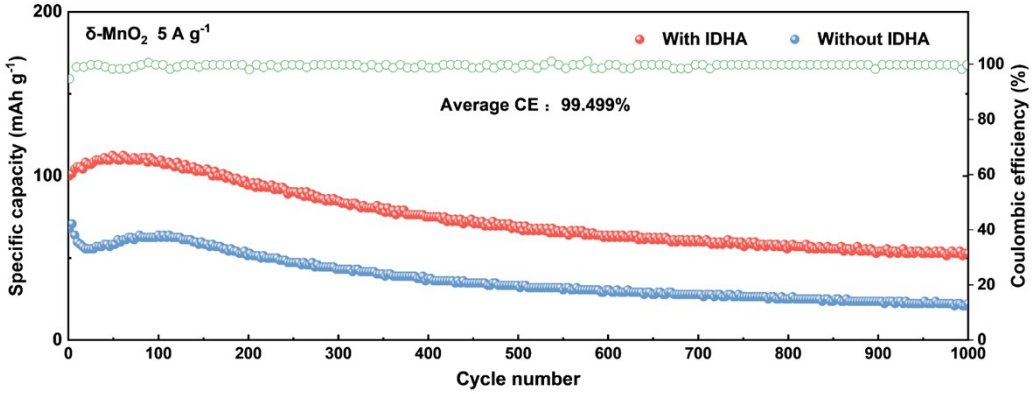

Fig. S27. Cycle testing of Zn//δ-MnO_2 full cells at a current density of 5 A g^{-1}.

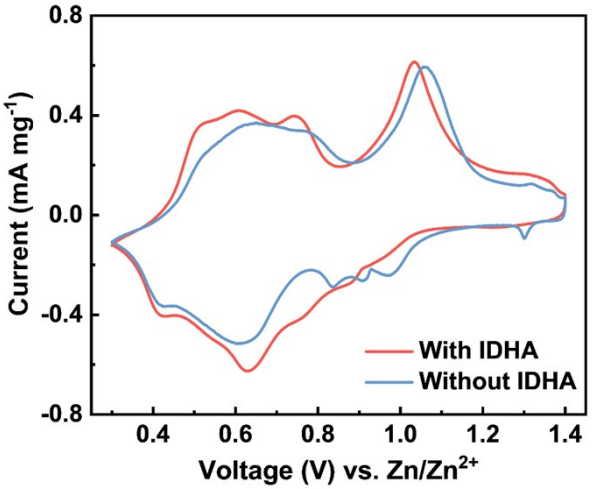

Fig. S28. CV testing of Zn//$NH_4V_4O_{10}$ full cells.

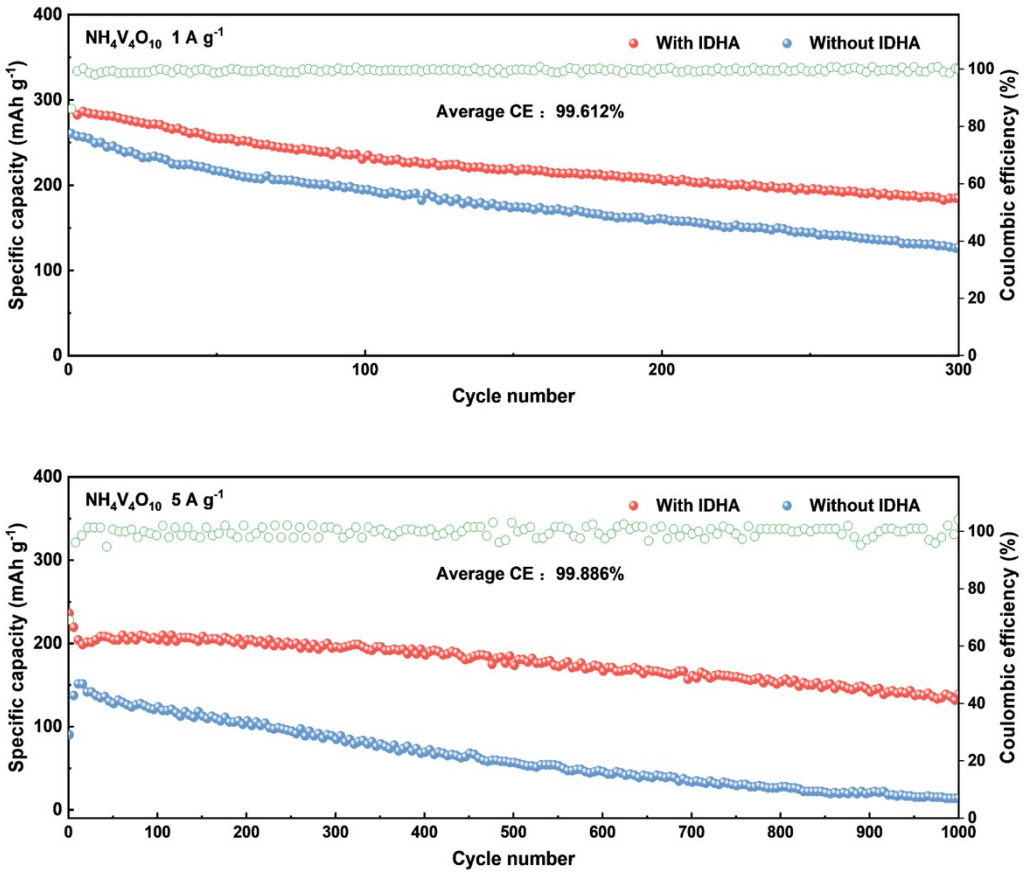

Fig. S29. Cycling performance of Zn//$NH_4V_4O_{10}$ full cell at 1 and 5 A g^{-1}

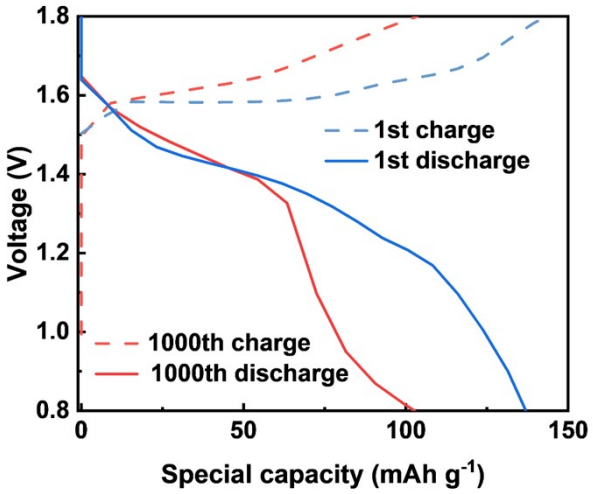

Fig. S30. The GCD curves of Zn//δ-MnO_2 pouch cells with IDHA additive at the first and 1000th cycle.

Fig. S31. The effect of different levels of folding on the voltage of pouch cells. Demonstrating the potential for flexible electronics applications.

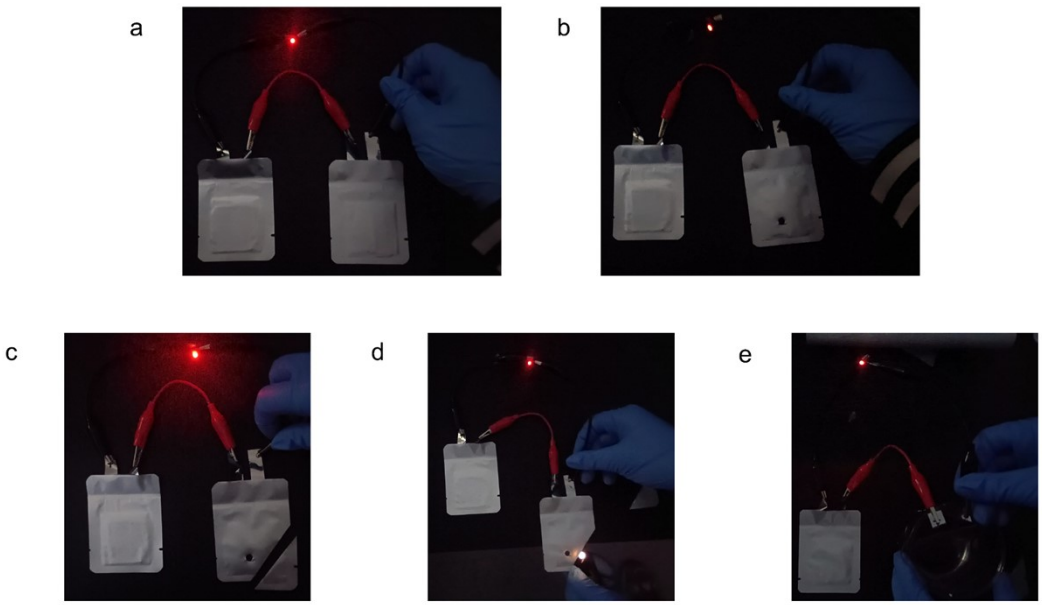

Fig. S32. Safety testing of pouch cells:a) Initial state b) Puncture c) Cutting d) Burning e) Immersion situation

Tab. S1. Performance comparison of symmetric Zn//Zn cells from the previously reported works involving electrolyte additives and our work.

Electrolytes	Current density/Areal capacity (mA cm^{-2}/mAh cm^{-2})	Lifespan (h)	CPC (Ah cm^{-2})	Refs.
2 M Zn SO_4+50 vol% PG	0.5/0.5	3500	0.875	[3]
	1/1	1000	0.5	
3 M $ZnSO_4$ in H_2O/68 vol% EG	0.5/0.5	2268	0.667	[4]
$ZnSO_4$+5 vol% NMP	1/1	540	0.27	[5]
$ZnCl_2$: $Zn(OAc)_2$ = 10:6	0.2/0.2	1200	0.12	[6]
2.5 M $Zn(OTf)_2$+0.04 wt% POV	0.5/0.25	1000	0.5	[7]
1:4 M Zn/Li-70:30 wt% PEG/H_2O	0.25/0.4	500	0.125	[8]
2 M $ZnSO_4$+0.0085 M $La(NO_3)_3$	1/1	1200	0.6	[9]
0.01 M $Ce_2(SO_4)_3$ in $ZnSO_4$	1/1	400	0.2	[10]
2 M $ZnSO_4$ in glycerol/water (50/50)	1/1	1500	0.9	[11]
	2/6	900		
2 M $ZnSO_4$+0.08 M ZnF_2	1/1	600	0.3	[12]
2 M $ZnSO_4$+5 mM vanilli	1/1	1000	0.5	[13]
1 M $ZnSO_4$+4 M EMImCl	1/1	500	0.25	[14]
1 M $ZnSO_4$+0.1 M TSC	5/1.25	200	0.5	[15]
3 M $Zn(CF_3SO_3)_2$+20 mM $Zn(NO_3)_2$	0.5/0.5	1200	0.3	[16]
7.6 M $ZnCl_2$+0.05 M $SnCl_2$	3/3	500	0.75	[17]
2 M $ZnSO_4$+1 vol% DME	2/2	380	0.38	[18]

3 M $ZnSO_4$+10 mM α-CD	5/5 10/1	200 160	0.5 0.8	[19]
2 M $ZnSO_4$+0.02 M IDHA	4/1	3430	6.86	This work

Reference

[1] J. Yin, R. Zhu, L. Xia, H. Liu, Y. Gao, Z. H. Gan, X. Feng, M. H. Wang, G. D. Meng, Y. Q. Su, Y. H. Cheng, X. Xu, J. Mater. Chem. A. 2023, 11, 11436-11444.

[2] B. Y. Tang, J. Zhou, G. Z. Fang, F. Liu, C. Y. Zhu, C. Wang, A. Q. Pan, S. Q. Liang, J. Mater. Chem. A. 2019, 7, 940-945.

[3] J. Li, S. Zhou, Y. Chen, X. Meng, A. Azizi, Q. He, H. Li, L. Chen, C. Han, A. Pan, Adv. Funct. Mater. 2023, 33, 2307201.

[4] R. Qin, Y. Wang, M. Zhang, Y. Wang, S. Ding, A. Song, H. Yi, L. Yang, Y. Song, Y. Cui, J. Liu, Z. Wang, S. Li, Q. Zhao, F. Pan, Nano Energy 2021, 80, 105478.

[5] T. C. Li, Y. Lim, X. L. Li, S. Luo, C. Lin, D. Fang, S. Xia, Y. Wang, H. Y. Yang, Advanced Energy Materials, 2022, 12, 2103231.

[6] M. Yang, J. Zhu, S. Bi, R. Wang, Z. Niu, Advanced Materials 2022, 34, 2201744.

[7] K. Yang, Y. Y. Hu, T. S. Zhang, B. Y. Wang, J. X. Qin, N. X. Li, Z. W. Zhao, J. W. Zhao, D. L. Chao, Adv. Energy Mater. 2022, 12, 2202671.

[8] D. E. Ciurduc, C. de la Cruz, N. Patil, A. Mavrandonakis, R. Marcilla, Energy Storage Mater. 2022, 53, 532.

[9] R. R. Zhao, H. F. Wang, H. R. Du, Y. Yang, Z. H. Gao, L. Qie, Y. H. Huang, Nat. Commun. 2022, 13, 3252.

[10] Y. Li, P. Wu, W. Zhong, C. Xie, Y. Xie, Q. Zhang, D. Sun, Y. Tang, H. Wang, Energy & Environmental Science 2021, 14, 5563.

[11] Y. J. Zhang, M. Zhu, K. Wu, F. F. Yu, G. Y. Wang, G. Xu, M. H. Wu, H. K. Liu, S. X. Dou, C. Wu, J. Mater. Chem. A 2021, 9, 4253.

[12] Y. An, Y. Tian, K. Zhang, Y. Liu, C. Liu, S. Xiong, J. Feng, Y. Qian, Adv. Funct. Mater. 2021, 31, 2101886.

[13] K. Zhao, F. Liu, G. Fan, J. Liu, M. Yu, Z. Yan, N. Zhang, F. Cheng, ACS Appl. Mater. Interfaces 2021, 13, 47650.

[14] Q. Zhang, Y. Ma, Y. Lu, X. Zhou, L. Lin, L. Li, Z. Yan, Q. Zhao, K. Zhang, J. Chen, Angew. Chem., Int. Ed. 2021, 60, 23357.

[15] N. Wang, S. Zhai, Y. Ma, X. Tan, K. Jiang, W. Zhong, W. Zhang, N. Chen, W. Chen, S. Li, G. Han, Z. Li, Energy Storage Mater. 2021, 43, 585.

[16] D. Li, L. Cao, T. Deng, S. Liu, C. Wang, Angew. Chem., Int. Ed. 2021, 60, 13035.

[17] L. Cao, D. Li, F. A. Soto, V. Ponce, B. Zhang, L. Ma, T. Deng, J. M. Seminario, E. Hu, X. Q. Yang, P. B. Balbuena, C. Wang, Angew. Chem., Int. Ed. 2021, 60, 18845.

[18] J. Cui, X. Liu, Y. Xie, K. Wu, Y. Wang, Y. Liu, J. Zhang, J. Yi, Y. Xia, Mater. Today Energy 2020, 18, 100563.

[19] K. Zhao, G. L. Fan, J. D. Liu, F. M. Liu, J. H. Li, X. Z. Zhou, Y. X. Ni, M. Yu, Y. M. Zhang, H. Su, Q. H. Liu, F. Y. Cheng, J. Am. Chem. Soc. 2022, 144, 11129.